

Sea surface currents and wind direction by VHF radar: results and validation

Véronique Cochin^{*†}, Philippe Forget[‡], Benoît Seille^{*} and Grégoire Mercier[†]

^{*}ACTIMAR, 24 quai de la douane, 29200 Brest - France

[†]GET-ENST Bretagne, CNRS UMR 2872 TAMCIC - Equipe TIME, CS 83818, Technopôle Brest-Iroise, 29238 Brest, France

[‡]LSEET Université de Toulon et du Var, CNRS 6017, BP 132, 83957 La Garde Cedex, France

Email: veronique.cochin@enst-bretagne.fr

Abstract—The performance and operational feasibility of the Very High Frequency (VHF) COSMER pulsed Doppler radar have been demonstrated in a region dominated by strong tidal currents. The VHF COSMER system was deployed in the Normand Breton Gulf (France) for the EPEL program, supported by the French Navy. Comparisons of ocean radial currents are made between these from COSMER system and these from an *in situ* instrument. We also made comparisons with currents simulated by the numerical model TELEMAC 2D. This paper presents results of the analysis. Preliminary results of wind direction estimation are also presented, using a \cos^s model.

I. INTRODUCTION

Shore-based High Frequency (HF) and Very High Frequency (VHF) radars (typically between 3 and 50 MHz) have, in the last 30 years, proved to be a very useful tool for understanding and analysing coastal circulation. Since Crombie's study on the backscattering of radio waves by the ocean surface [1], the principle underlying the HF Doppler radar techniques has been investigated theoretically [2] [3]. This concept of measurements received considerable attention in coastal oceanographic experiments in order to extract in quasi real time information about oceanographic parameters, such as sea surface current velocities, wave spectrum and wind direction [4] [5]. The main advantage of remote sensing methods is to provide measurements over a large scale (thousand of kilometres), with high spatial and temporal resolution (one measurement every 30 minutes, down to 10 minutes). This makes it possible to track oceanographic phenomena, which is not possible with moored instruments such as ADCP which provides the variation of a parameter over time at a given point. HF radars do not provide global coverage like the well known satellite based system but they have the advantage of giving a continuous observation in limited areas with high spatial resolution (from a few kilometres to a few hundred metres) and with high temporal resolution compared with a repeat cycle of several days for satellite systems. Also, computed maps of surface current vectors are particularly useful for the validation and calibration of numerical hydrodynamic models, because the models produce averaged currents over the water column and over grid spaced pixels in the same way as current maps.

For these systems, propagation mainly occurs by ground wave propagation and radio waves are backscattered by the moving ocean surface gravity waves. Measurements are achieved through the Doppler spectrum of the radio waves backscatter signal, using the Bragg scattering principle. Bragg scattering is a coherent reflection of energy transmitted by ocean surface waves. First order scatter from specific spectral components of the ocean wave field produces the dominant contribution. These components, termed *Bragg waves* have a wavelength λ_{wave} exactly one-half the transmitted radar wavelength λ_{radar} and are moving radially away from or toward the radar. They produce two dominant peaks in the echo Doppler spectrum which are symmetrically positioned about the radar frequency. These peaks are displaced according to the phase velocity of the surface waves $v_{\text{wave}} = \omega/k_{\text{wave}}$, where $\omega^2 = gk$ is the linear dispersion relationship in deep water (g is the acceleration due to gravity and k is the wavenumber). In the absence of ocean currents, the Doppler frequency shift always occurs at a known theoretical position in the frequency spectrum, which depends only on the radar transmitter frequency. This frequency is called the *Bragg frequency*, given by $f_B = \sqrt{g/(\lambda_{\text{radar}}\pi)}$. If there is a surface current, the returned signal exhibits a Doppler-frequency shift Δf from the theoretical position. This shift, which is the difference between the theoretical and the observed Doppler frequency, is related to the radial component of the effective surface current, moving toward or away from the radar by $\Delta v = \lambda_{\text{radar}}\Delta f/2$. The rest of the power spectrum comprises a continuum, referred to as the second order part of the spectrum, and a noise floor. The sidebands surrounding the Bragg peaks are due to non linear wave-wave interactions and higher order Bragg scatter. The second order scatter contains the most significant portion of the ocean wave energy information. Several approaches have been developed to provide a theoretical formulation for relating the Doppler spectrum of the backscatter cross section to the complete ocean wave directional spectrum. Techniques of inversion of the second order equation are used to extract the two dimensional wave height spectrum [4]. Wind information can be extracted by analysing the Doppler spectrum. The ratio R of energy densities in the two first order peaks gives information about wind direction when used simultaneously

with a method describing the directional distribution of the waves. This method can be either a model (for example $A \cos^s[(\theta_{\text{radar}} - \theta_{\text{wind}})/2]$ with $s = 4$ is often used) [6] [7] [8] or a semi-empirical relationship between the ratio and wind direction [9]. Wind speed can be estimated using second order terms or by using a multi-frequency radar [10].

In this paper, we will present an analysis of VHF COSMER radar measurements acquired in a strong tidal current area. Sea surface radial currents have been compared with current acquired by an *in situ* instrument and with numerical simulations obtained by a 2D model. The results show differences, which may be explained by vertical current shear and horizontal variability in this particular point of measurements. Preliminary results on the estimation of wind direction are also presented. This paper is organised as follows: in section II, we describe the experiment and the different sources of data acquired and used for this work. In section III, we present the method used to make comparisons between radar measurements, *in situ* data, and numerical simulations and the method used to estimate wind direction. In section IV we present results of current comparisons and preliminary results obtained to extract wind direction from the VHF radar measurements.

II. EXPERIMENT

In this study, we used VHF COSMER data acquired during the EPEL program (*Evaluation et Prévision de l'Environnement Littoral*), supported by the French Navy, in the Normand Breton Gulf (France). The VHF COSMER system has been developed by the *Laboratoire de Sondages Electromagnétiques de l'Environnement Terrestre* (LSEET) group (University of Toulon, France) [11]. This system includes two pulsed Doppler radars (45 MHz and 47.8 MHz respectively) to map coastal sea surface currents over a large area, of about 25 km by 25 km. During the EPEL program, this system was deployed in operational mode and the radars operated with a pulsed width of $4 \mu\text{s}$ determining a range resolution of 600 metres (possibility of 150 metres with this radar) and a pulse repetition rate of $200 \mu\text{s}$ (maximum range: 30 km). Each station used a linear phased array for the receiving network and beam forming processing to produce an effective 3 dB beam width of 14 degrees (azimuth resolution) [12]. The receiving network had 8 whip antennas parallel to the coast (total length: 25 m or 50 m if 16 antennas used) and the transmitting network had 4 whip antennas perpendicular to the coast (total length: 12 m).

Both radars measure the radial components of the current in the range direction, at all the sampled distances. Each radar derives a vertically averaged quantity over 25 cm (at 50 MHz) and temporally averaged over 9 minutes. The radar data obtained after real time signal processing consists of the 256 points Doppler spectra, calculated by the Fast Fourier Transform (FFT) algorithm [13]. Figure 2 represents a typical spectrum obtained by the VHF COSMER radar during the EPEL experiment (45 MHz radar frequency; 6.6 m radar wavelength; 3.3 m Bragg wave wavelength, 0.7 Hz Bragg frequency). First order lines and the Doppler shift Δf are

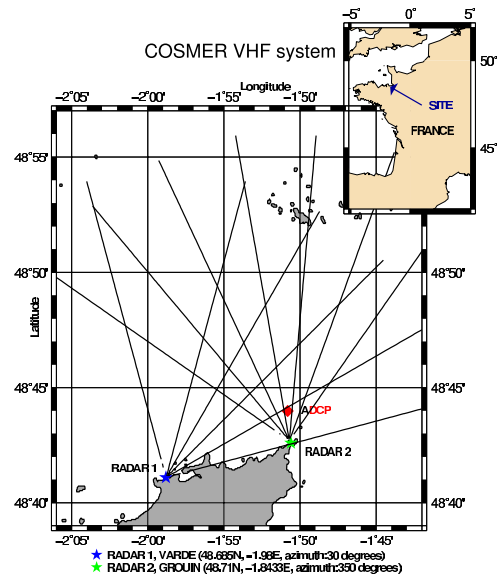


Fig. 1. Observation sites during the EPEL-GNB experiment in the Normand Breton Gulf, France. The VHF COSMER stations are marked with stars. ADCP is the *in situ* instrument, which acquired current measurements simultaneously with the radar.

indicated. The eastward and northward components of ocean currents are estimated on a 1 by 1 km grid, combining the two radial components. The description of the VHF COSMER radar characteristics during the EPEL experiment are given in Table I. Measurements were acquired continuously every 30 minutes for 28 days in February - March 2003, including the high spring tide. The database contains 2688 samples, coming from the two radar stations. A few data are missing for radar 1 (Varde) on March 5, 2003.

During the EPEL experiment, *in situ* instruments such as ADCP (*Acoustic Doppler Current Profiler*) and current metres were moored on the bottom of the sea (depth around 20 m). In this paper, we used measurements acquired by the instrument AWAC from NORTEK, deployed at position $48^{\circ}44,01\text{N}$, $1^{\circ}50,498\text{W}$ (noted ADCP in Fig.1). Measurements were collected at ten minute intervals with an average interval of 2 minutes, from February, 8 to March 11, 2003. The instrument was adjusted to make Doppler measurements into 28 vertical bins, each with a length of 1 m. Each measurement represents current integrated over two bins (2 m). The analysis of the vertical profile of the current, considering all the bins of the ADCP, showed noisy data. We thus chose to average measurements over two bins. The shallowest bin without contamination due to surface reflections (which includes the blind zone of the instrument) was found to be 4 m below the sea surface.

Wind data were obtained by SHOM (*Service Hydrographique et Océanographique de la Marine*, French Navy)

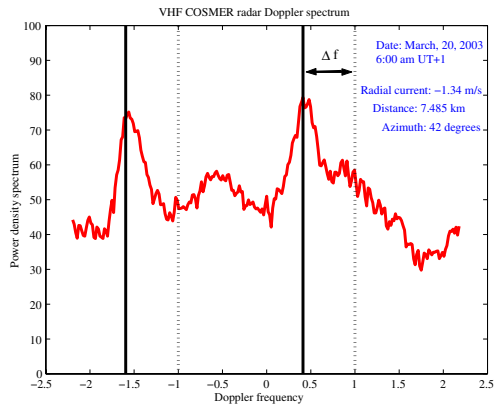


Fig. 2. Typical radar sea echo spectrum from VHF COSMER radar (EPEL Program) showing the Doppler-shifted peaks away from the theoretical position of the radar Bragg peaks.

TABLE I
VHF COSMER SYSTEM CHARACTERISTICS IN OPERATIONAL MODE
DURING EPEL-GNB PROJECT.

Radar COSMER	
Radar type	Pulse
Operating frequency	45 MHz / 47 MHz
Wavelength	6.66 m / 6.27 m
Length of sea surface wave (Bragg)	3.33 m / 3.13 m
Frequency of Bragg wave	0.68 Hz / 0.70 Hz
Average power	30 W
Pulse repetition rate	200 microseconds (5 kHz)
Pulse length	4 μ s (possible 1 μ s)
Radial resolution	600 m (possible 150 m)
Range	30 km
Depth over which current is averaged	0.25 m ($\lambda_{\text{radar}} / 8\pi$)
Doppler spectrum processing	FFT: 256 points, Sampling frequency: 3 Hz, Frequency resolution: 0.01 Hz
Integration time	9 minutes
Antennas	
Transmit network (<i>end-fire</i>)	4 whip antennas $\lambda_{\text{radar}}/4$ beam width: 90 degrees (-3 dB)
Receive network (<i>broadside</i>)	8 whip antennas $\lambda_{\text{radar}}/4$ spacing $\lambda_{\text{radar}}/2$
Azimuthal resolution (beam forming)	+/- 7 degrees (-3 dB)

to perform this analysis. Records came from a meteorological station located on shore at Dinard, almost ten kilometres South-West from radar 1 site (Fig.1). Wind speed and direction were given every hour.

III. METHOD

A. Currents comparison

In order to validate sea surface current measurements obtained by the VHF radar in strong tidal areas, we made comparisons with other sources of current data: the subsurface currents obtained by ADCP and simulations from the hydrodynamical numerical model TELEMAC 2D. The method

is the same for both comparisons (radar versus ADCP and radar versus numerical model): we chose to compare the time series of radial components instead of vectors in order to avoid additional error due to the geometry between radar beams when calculating the current vectors. Thus, ADCP measurements and numerical simulations were rotated over the corresponding radar beam for the two radar sites.

The numerical method makes use of the hydrodynamic model TELEMAC 2D. This model calculates averaged currents over the water column on mesh nodes. In previous work [12], we compared the tidal currents extracted from the radar to that simulated by SHOM to edit two dimensional tidal streams maritime maps. We made use of a hodograph representation over both neap tide and high tide cycles, which can be more readable and accessible for maritime users. In this present work, we had the model run for the specific period of measurement time and over specific location points. In this paper we present the results obtained at the point noted ADCP in Fig.1.

ADCP measurements, integrated over 2 minutes, were averaged over ten minutes (two interval measurements), to better fit the radar measurements which are integrated over 9 minutes. Radar measurements were low-pass filtered to smooth the time series. For radar 2 (Grouin), the *in situ* instrument is in a measurement cell close to the coast and at this location, in the eastern direction, certain abnormal behaviour in the Doppler spectra appeared, mainly due to side lobes in the antenna pattern and in presence of sea water (Mont Saint Michel Bay). For radar 1 (Varde), the *in situ* instrument is 11.2 kilometres away and the radar surface cell is around 1.9 km². In this paper, we will present only radial comparisons made with radar 1 (Varde).

B. Wind direction estimation

Following the theory developed by Barrick [14] on the backscattered electromagnetic wave over the sea surface, the radar cross section in the Doppler frequency domain is given by:

$$\sigma_1(\omega) = 2^6 \pi k_0^4 \sum_{m=\pm 1} S(-2mk_0) \delta(\omega - m\omega_B) \quad (1)$$

where $S(k)$ is the directional wave spectrum, k_0 is the radar wavelength, ω_B is the frequency shift of the first order lines and the Dirac delta function δ is the constraint for first order line frequencies. Several ocean surface wave models can be found on the literature and are discussed in [15].

Using Eq.1, the spectral energy density of Bragg peaks ($\sigma_1(\omega_B)$ and $\sigma_1(-\omega_B)$ for approaching and receding Bragg waves respectively) is a function of the sea wave spectrum. Using the angular function $G(\theta)$ of the wave spectrum ($S(k) = F(k)G(\theta)$, where the maximum is in the direction θ) and the ratio of Bragg peaks, the omnidirectional wave spectrum $F(k)$ is cancelled and Eq.(1) becomes:

$$\frac{\sigma_1(\omega_B)}{\sigma_1(-\omega_B)} = \frac{G(\pi - \theta)}{G(\theta)} \quad (2)$$

where θ represents the wind direction relative to the radar line of sight ($\theta = \theta_{\text{wind}} - \theta_{\text{radar}}$). The Bragg peak ratio gives information about the directional properties of Bragg waves. Assuming that gravity waves are wind generated, the wind direction can be estimated by using both this ratio and a method describing the directional distribution. The difficulty lies in estimating the appropriate model [7] [8].

In this analysis, we used the cardioid directional model defined by:

$$G(\theta) = \frac{\epsilon + (1 - \epsilon)\cos^s \frac{\theta}{2}}{N(s)} \quad (3)$$

where s is the spreading parameter, a function of wind speed and waves (for high values of s , waves are more directive), $N(s)$ is a normalization factor and ϵ is a fraction of wave energy travelling against the wind direction (quantity much less than 1) [6] [16]. There is an ambiguity about estimating wind direction if using a single look angle radar because it can be either clockwise or counterclockwise relative to the radar beam. This ambiguity is resolved by using two radar beams looking at the same position by solving:

$$\min \left(\sum_{i=1,2} \left[R_i - \frac{G(\pi - \theta)}{G(\theta)} \right]^2 \right) \quad (4)$$

where i denotes the radar site and R is the Bragg peak ratio.

In this work, we analysed statistically the ratio of first order Bragg peak densities, over all the radar cells (distance and azimuth) and over a one month period for both radars. In order to avoid inhomogeneity due to the condition of high variability in relative wind (influence of strong tidal currents in low wind speed), wind speed should be greater than current speed [17]. In the area of measurements, we observed strong tidal currents, greater than 2 m.s^{-1} . We selected a period of high wind speed, greater than 5 m.s^{-1} , and three hours for stationarity in wind direction, which is more than the time delay for the peak of the wave spectrum to reach a new equilibrium after a wind change [16]. In these cases, we consider that wind has a speed high enough to saturate the waves responsible for the first order echo in the radar Doppler spectrum. Indeed, considering that the wavelength at the peak of the wave spectrum depends on the wind speed at ten metres ($\lambda_p = 2\pi U_{10}^2/g$) [18], Bragg wave wavelengths are shorter when wind speed is greater than 2.8 m.s^{-1} (VHF COSMER: 45 MHz radar frequency; 3.3 m Bragg wave wavelength, 0.7 Hz Bragg frequency). Also, in the case of limited fetch (for example, if the wind is blowing from the South) and following an empirical power law relating the inverse wave age to the dimensionless fetch X (which depends on wind speed when limited) given by Hasselman et al. [16] $\Omega_c = 22X^{-0.33}$, where $X = gx/U_{10}^2$ and x is the distance in metres, we found that our limits give the period of a mature (Ω_c close to 1) or fully developed sea (Ω_c close to 0.84).

We then used all the data set (measurement cells in distance, azimuth and time) of the selected period to perform a statistical analysis. These data were used to estimate ϵ , which

corresponds mostly to the maximum negative value of the Bragg peak ratio (direction of zero degrees), averaged over 10 degrees. We found a value of 0.025. Then, the value of s is empirically estimated to fit the data, as shown in Fig.6.

IV. RESULTS

A. Currents comparison

The radial components of sea surface current measured by the radar and those measured by the *in situ* instrument are shown in Fig.3 for site 1 (Varde). At the top we represent the time series and in Fig.4 we represent the histogram (top) and scatter plots of more than 625 points (almost 1 point every 30 minutes and a period of missing data for radar 1 on March 5). We found a good correlation coefficient of 0.97 and an offset of around 20 centimetres. Results of statistical analysis are given in Table II, with corresponding coefficients for the linear regression line. We found higher currents measured by the ADCP. Observed differences are mainly due to techniques of acquisition [19]. The electromagnetic method yields a spatially and temporally averaged surface current measurement and is limited to observation near the sea surface, whereas the acoustic method produces a subsurface point measurement into bins of the water column. In addition, higher time integration and temporal resolution might smooth the currents (which can change rapidly, particularly in spring tides). Sea surface current measured by radar also includes both the surface Stokes drift and the Eulerian current, according to the limit of the accuracy of the method [20]. In previous work, we found an Eulerian current in the order of 20 cm.s^{-1} , depending on wind conditions [12]. Differences can also be explained by geophysical variability, especially close to the coast (ADCP position), where currents are important and spatially variable (horizontal and vertical). This variability is mainly due to the bathymetry and the presence of a channel, between the cape and the island, near radar 2 (Grouin) as shown in Fig.5. This figure represents the simulation of current speed on March 3, 2003, over the area of radar measurements, without (at the top) and with (at the bottom) the presence of the island, which creates a channel with high current speed in the South - North direction. This simulation is made at high tide plus 3 hours, where tidal currents are strong (maximum for ebb tide).

The radial components of simulated currents are represented as a time series in Fig.3 (bottom). Figure 4 shows histograms and scatter plots obtained for this comparison. We found for the radial of radar 1 a correlation coefficient of 0.98 and a slope for the linear regression line of 0.878. Graphs with the numerical model show under-estimated currents, but this can be explained because the simulation represents currents averaged over the water column.

B. Wind direction estimation

Figure 6 represents the dispersion of averaged Bragg peak ratio (in dB) versus wind direction relative to radar line of sight (in degrees) and the curve corresponding to the cardioid model (Eq.3) for $s = 7$ and $\epsilon = 0.025$. According to this figure, the precision on wind direction varies with the wind

TABLE II

STATISTICS ON MEASUREMENTS OF RADIAL FROM VHF COSMER RADAR AND ADCP AND TELEMAC 2D DURING EPEL-GNB PROJECT.

1	2	3	4	5	6	7	8	9	10
Radar Site	data	min (m.s ⁻¹)	max (m.s ⁻¹)	avg (m.s ⁻¹)	std (m.s ⁻¹)	ρ	ΔV_{RMS}	$\Delta bias$	Linear regression
Varde		-1.269	0.957	-0.019	0.539				
	ADCP	-1.342	0.886	-0.105	0.578	0.933	0.209	0.087	$V_{RADAR} = 0.869V_{ADCP} + 0.073$
	TELEMAC	-1.292	0.854	0.009	0.645	0.945	0.222	-0.027	$V_{RADAR} = 0.790V_{TELEMAC} - 0.026$

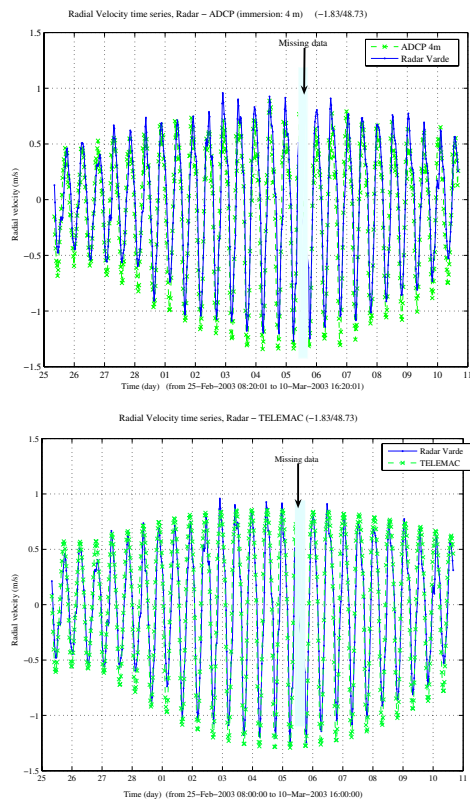


Fig. 3. Top: time series of radial current components from radar 1 (Varde) and *in situ* measurements. Bottom: time series of radial current components from radar 1 (Varde) and simulated data from TELEMAC 2D.

direction itself. For example, a 4 dB variation on the Bragg ratio amplitude corresponds to a greater variation in wind direction for a high Bragg peak ratio (around 40 degrees) than for a small Bragg peak ratio. Following Eq.4, wind direction was estimated on a point located to the north of the meteorological station, where the smallest limited fetch is around 15 kilometres (South-East) at position 48°49N, 1°58.5W. Results, given in Fig.7 show good agreement with the measured wind direction.

V. CONCLUSION AND PERSPECTIVES

We found a good correlation coefficient between the radial components measured by the radar and those from the *in situ* instrument. Comparisons with simulations show that the current is under-estimated by the model. Simulations over the radar coverage show a high variability in the coastal area, which may explain the difference observed between

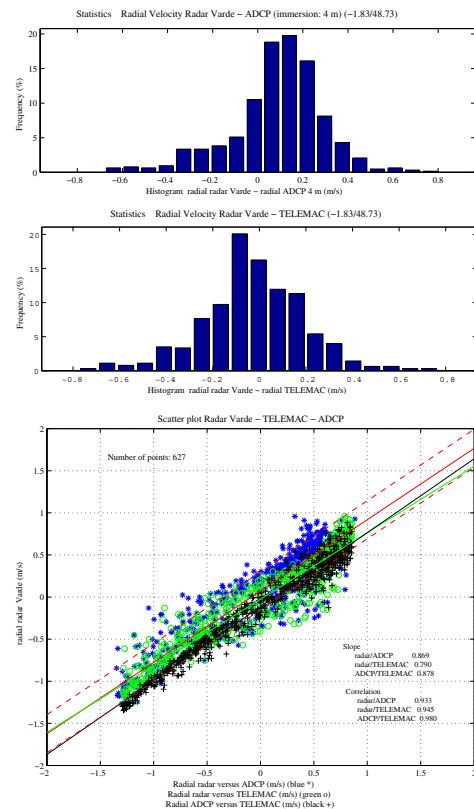


Fig. 4. Top: Histograms for current component differences between radar 1 - ADCP (top) and radar 1 - TELEMAC 2D. Bottom: scatter plots for current components of radar versus ADCP, radar versus TELEMAC, and ADCP versus TELEMAC.

the measured data. In preliminary work on wind direction estimation, we first defined a wind speed threshold because relative wind at low speed can be modulated by strong tidal currents, and thus can change rapidly. We selected a high speed period of time to estimate an averaged model for wind direction estimation. As the precision of the model depends on wind direction, this model can be used if a change in wind field direction is greater than the precision, otherwise, it will not be detected. Further work still has to be done in order to improve the accuracy of the model.

ACKNOWLEDGEMENT

The authors gratefully acknowledge Pierre Broche (LSEET) for his support in data analysis and SHOM, particularly Fabrice Arduin, Ronan Le Roy, Bernard Simon, Lucia Pineau, Michel Le Goff and Michel Aidonidis for providing data sets.

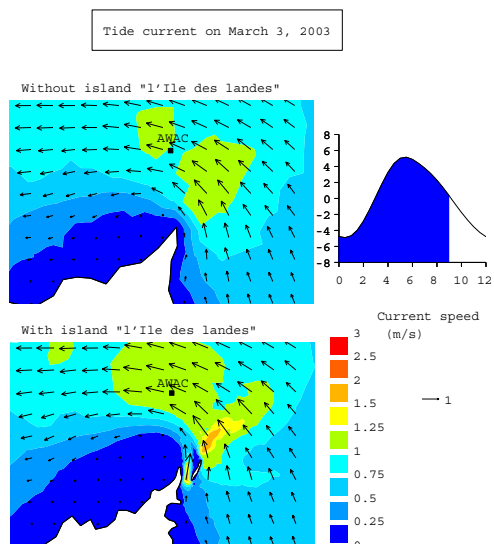


Fig. 5. Current simulations on March, 3 2003 at high tide plus 3 hours, over radar measurement area, showing high spatial variability in the coastal area, mainly due to the influence of the bathymetry. Top: without presence of the island, near radar 2 (Grouin). Bottom: with the island.

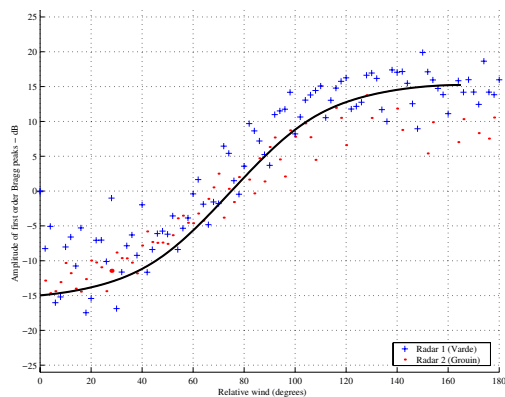


Fig. 6. Dispersion of averaged Bragg peak ratio (in dB) versus wind direction relative to radar line of sight (in degrees), over the total period of measurements (1 month).

We also wish to thank *Conservatoire de l'espace littoral et des ravages lacustres, Conseil général de l'île et Vilaine* and local authorities for authorisation in radar settings.

REFERENCES

- [1] D. D. Crombie, "Doppler spectrum of sea echo at 13.56 mc/s," *Nature*, vol. 175, no. 4459, pp. 681–682, April 1955.
- [2] D. E. Barrick, "First-order theory and analysis of MF/HF/VHF scatter from the sea," *IEEE Trans. Antennas Propagat.*, vol. 20, no. 1, pp. 2–10, January 1972.
- [3] D. E. Barrick, M. W. Evans, and B. Weber, "Ocean surface currents mapped by radar," *Science*, vol. 198, pp. 138–144, 1977.
- [4] L. R. Wyatt, "Limits to the inversion of HF radar backscatter for ocean wave measurement," *Journal of Atmospheric and Oceanic Technology*, vol. 17, pp. 1651–1665, December 2000.
- [5] K. W. Gurgel, H. H. Essen, and S. P. Kingsley, "High-frequency radars: physical limitations and recent developments," *Coastal Engineering*, vol. 37, no. 3-4, pp. 201–218, August 1999.

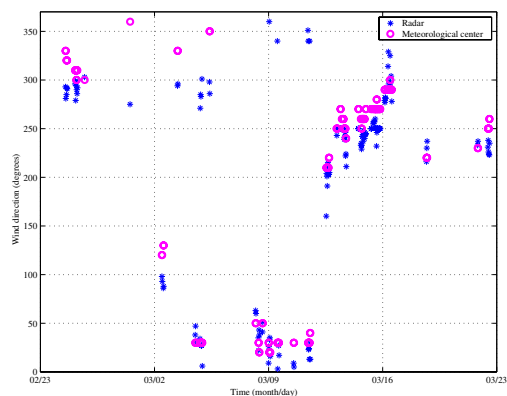


Fig. 7. Wind direction estimated by VHF COSMER measurements and those measured by the meteorological station.

- [6] M. S. Longuet-Higgins, D. E. Cartwright, and N. D. Smith, "Observations of the directional spectrum of sea waves using the motions of a floating buoy," *Ocean Wave Spectra*, Prentice-Hall, Englewood Cliffs, New Jersey, pp. 111–132, 1963.
- [7] M. L. Heron and R. J. Rose, "On the application of HF ocean radar to the observation of temporal and spatial changes in wind direction," *IEEE Journal of Oceanic Engineering*, vol. 11, no. 2, pp. 210–218, April 1986.
- [8] L. R. Wyatt, L. J. Ledgard, and C. W. Anderson, "Maximum likelihood estimation of the directional distribution of 0.53 Hz ocean waves," *Journal of Atmospheric and Oceanic Technology*, vol. 14, pp. 591–603, June 1997.
- [9] A. E. Long and D. B. Trizna, "Mapping of north atlantic winds by HF radar sea backscatter interpretation," *IEEE transactions on antennas and propagation*, vol. 21, no. 5, pp. 680–685, September 1973.
- [10] J. F. Vesecky, L. A. Meadows, Y. M. Fernandez, C. C. Teague, J. M. Daida, J. R. Paduan, R. del Gado, and P. E. Hansen, "HF radar observations of wind-current relationships at the air-sea boundary," in *IGARSS'99*, vol. II, 1999, pp. BBC02.11.1–BBC02.11.3.
- [11] P. Broche, J. C. Crochet, J. C. De Maistre, and P. Forget, "VHF radar for ocean surface current and sea state remote sensing," *Radio Science*, vol. 22, pp. 69–75, 1987.
- [12] V. Cochon, V. Mariette, A. Coat, P. Broche, J. C. De Maistre, Y. Barbin, J. Gaggelli, G. Mercier, and R. Garello, "Tidal analysis and currents mapping using VHF radar and ADCP measurements in the Normand Breton Gulf - france," in *OCEANOPS 2004 proceedings*, 2004.
- [13] D. Barrick, "Accuracy of parameter extraction from sample averaged sea echo doppler spectra," *IEEE transactions on antennas and propagation*, vol. 28, no. 1, pp. 1–11, January 1980.
- [14] —, *Remote sensing of sea state by radar*. NOAA/Environmental Research Laboratories, 1972, ch. 12 of Remote Sensing of the Troposphere, pp. 12.1–12.6.
- [15] T. Elfouhaily, B. Chapron, K. Katsaros, and D. Vandemark, "A unified directional spectrum for long and short wind-driven waves," *Journal of Geophysical Research*, vol. 102, no. C7, pp. 15 781–15 796, 1997.
- [16] D. E. Hasselman, M. Dunckel, and J. A. Ewing, "Directional wave spectra observed during JONSWAP 1973," *Journal of Physical Oceanography*, vol. 10, pp. 1264–1280, 1980.
- [17] P. Forget, P. Broche, and J. C. De Maistre, "Attenuation with distance and wind speed of HF surface waves over the ocean," *Radio Science*, vol. 17, no. 3, pp. 599–610, May-June 1982.
- [18] M. L. Heron, "The effect of bimodal sea spectra on HF radar wind analysis," in *IEEE Oceans04*, 2004.
- [19] H. C. Graber, B. K. Haus, R. D. Chapman, and L. Shay, "HF radar comparisons with moored estimates of current speed and direction: Expected differences and implications," *Journal of Geophysical Research*, vol. 102, no. 8, pp. 18,749–18,766, August 1997.
- [20] P. Broche, J. C. De Maistre, and P. Forget, "Mesure par radar décimétrique cohérent des courants superficiels engendrés par le vent," *Oceanologica Acta*, vol. 6, pp. 43–53, 1983.